Presented at the OE/Aerospace
& Remote Sensing SPIE Conference
Orlando, FL April 1993
(Paper 1945-26)

Performance of the FOS detectors in a variable external magnetic field

W. A. Baity, E. A. Beaver, R. D. Cohen, V. T. Junkkarinen and R. W. Lyons

University of California, San Diego
Center for Astrophysics & Space Sciences, 0111
9500 Gilman Drive
La Jolla, California 92093-0111

J. E. Fitch and G. F. Hartig

Space Telescope Science Institute
3700 San Martin Drive
Baltimore, Maryland 21218

D. J. Lindler

Advanced Computer Concepts, Inc.
11518 Gainsborough Rd.
Potomac, Maryland 20854

ABSTRACT

We present the results of an investigation of the in-orbit performance of the Digicon detectors in the Faint Object Spectrograph (FOS), conducted as part of the commissioning phase of the Hubble Space Telescope. This paper includes orbital results on detector background noise, sensor image stability, and photometric stability along with several typical FOS observations. This information should be of general interest to designers of future spacecraft detectors and to astronomers observing with the FOS instrument.

1. INTRODUCTION

The Faint Object Spectrograph[1] (FOS) is one of five science instruments aboard the 2.4 meter Hubble Space Telescope. As the name implies, the FOS is designed to make spectroscopic observations of faint astronomical objects, often located at the outer limits of the universe. FOS modes of operation include coarse two dimensional imaging for target acquisition purposes, spectroscopy at low (R=220) and moderate (R=1200) resolution, along with spectropolarimetry at these resolutions. The FOS contains two photon counting detectors. The "Blue" Digicon covers the wavelength range from 1200Å to 5600Å with optimized performance shortward of 1600Å. The "Red" Digicon covers the 1600Å to 8500Å wavelength region with optimized performance longward of 1700Å.

Although Digicon detector was invented[2] over 20 years ago, it was one of the first photon-counting camera tubes specifically designed for space astronomy applications such as the HST[3]. Before these detectors were selected for use on the HST in the FOS and Goddard High Resolution Spectrograph (GHRS) instruments in 1977, 40-channel and 200-channel Digicon versions were set up at various ground-based telescopes in order to refine the design for the HST application by performing astronomical research[4]. Design and fabrication[5] of the FOS instrument occurred from 1978 to 1982 with instrument ambient and thermo-vacuum calibration[6] occurring in 1983. At contract award in 1978 the HST was scheduled for launch in late 1983; however delays, the most serious being associated with the Challenger accident in 1986, caused the Space Shuttle launch of the HST to slip to 1990.

In April 1990, the Hubble Space Telescope (HST) was launched into a near-circular, 610 km altitude, 28.5° inclination orbit. After 45 days in orbit, the FOS instrument had sufficiently outgassed at 5×10^{-5} Torr to safely command the

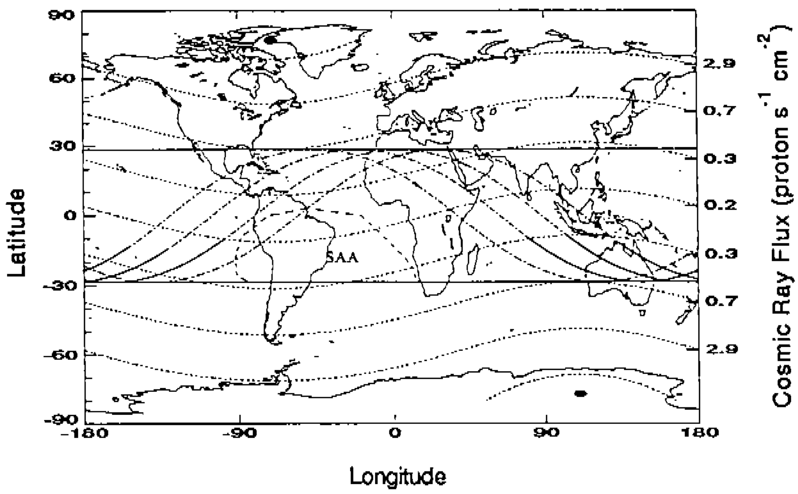

Figure 1. HST orbital plot of UM675 observation

FOS Digicon detectors to their negative 22,000 volt operating voltage. In this article we discuss those aspects of the FOS detector performance associated solely with orbital operations. The ground test data for the FOS flight Digicon detectors have been reviewed previously[7]. The data that we analyze here comes from the 18-month commissioning phase of HST observations, termed Science Verification (SV). During this SV period the HST was calibrated for science operations and numerous early science observations were performed. After some 3 years in orbit the FOS instrument remains fully operational and is the most frequently requested instrument by general observers for scientific studies on the HST.

Figure 1 illustrates the orbits of a typical HST science observation. This HST early science observation on the faint Quasi Stellar Source (QSO) UM675 took a total of 100 minutes divided among the illustrated three successive orbits. The solid line sections on the dot-dashed orbital tracks on Figure 1 are the three 2000 second segments of the UM675 observation. Generally long observations with the HST must be broken into sections because of periodic interruptions such as earth occultation and passage through the South Atlantic Anomaly (SAA) radiation field.

Throughout the HST orbit, variations in temperature, high energy particle radiation, plasma flux, and magnetic fields all contribute to a dynamically changing environment in which consistent and optimal detector performance must be maintained. In section 2 we review the FOS detector design with particular emphasis on those features designed to suppress detector orbital effects.

As the HST orbits, the Earth's dipole magnetic field produces a changing external magnetic field in the FOS reference frame. The character of the earth's dipole field in the FOS reference plane is a sinusoidal-like variation at about 2 cycles per orbit. Although peak-to-peak amplitude variation of the field is dependent on HST pointing direction and orbit geometry, the worst case peak-to-peak amplitude variation of the HST orbit is about 0.5 gauss in the FOS frame. Any penetration of this field into the interior of an electron tube type detector such as the Digicon leads to a geomagnetically induced motion of the electrons. In section 3 we describe the performance of the FOS detectors in the Earth's magnetic field and present a novel new technique to remove its influence on electron tube type detectors.

The major radiation field affecting the FOS detectors during HST science observations is the cosmic ray flux of average energy 8×10^{9} eV, varying from a minimum of roughly 0.2 protons s^{-1} cm^{-2} at 0° geomagnetic latitude to ~5 protons s^{-1} cm^{-2} at 90° geomagnetic latitude, using the worst case solar minimum values[8]. Lines of constant geomagnetic latitude are plotted every 20° as dotted lines in Figure 1; the geomagnetic poles are shown as large spots in Figure 1. The maximum geomagnetic latitude for the HST orbit is 39.9° (28.5° plus the 11.4° offset of the geomagnetic pole from the rotational pole). Since cosmic ray flux depends primarily on geomagnetic latitude and increases towards the geomagnetic poles, one can see from Figure 1 that for the HST orbit, cosmic ray flux peaks over Florida and Australia at 0.7 protons s^{-1} cm^{-2}. Fortunately, the low latitude and altitude of the HST allow the Earth's magnetic field to screen a significant fraction of the incident cosmic ray flux. Passage of these comic rays through the FOS detector leads to Cerenkov light flashes in the detector faceplate. In section 4 we discuss the effect of cosmic rays on the FOS detector background and a software technique for suppressing burst noise.

The other radiation field incident on the HST is due to the dip in the Earth's Van Allen radiation field centered over the south Atlantic off Brazil (the SAA in Figure 1). During each day, 7 of 15 HST orbits transit this high energy flux of protons and electrons. For an orbit of maximum SAA penetration, the HST is within the SAA contour for about 20 minutes of the 96 minute orbital period. The proton flux in the SAA core for E>50MeV is expected to peak at about 2000 protons s^{-1} cm^{-2} for the 610 km HST altitude. Protons of significantly lower energy as well as most electrons should not be able to reach the detector, since the structure of the HST will act to shield out these particles. Over a three year period of time, the FOS detector radiation dose due to SAA encounters is expected to be around 1000 rad. At this level of irradiation, detector lifetime degradation effects such as faceplate darkening and amplifier gain reduction can develop with time. This issue is covered under the section 5 topic of FOS photometric stability.

2. FOS DIGICON DETECTORS

The two FOS Digicon detectors differ only in their faceplate material and photocathode composition. The "Blue" Detector has a semitransparent sodium bialkali photocathode deposited on a MgF window, whereas the "Red" detector has a semitransparent trialkali photocathode deposited on a Suprasil (quartz) window. Figure 2 illustrates the FOS detector layout. Several features of the FOS detector design suppress the degrading influence of the orbital environment on detector performance.

The FOS detectors are controlled by a dedicated 16-bit microprocessor with 64 kilobits of memory. This allows most detector functions to be adjusted in order to optimally perform scientific studies and minimize the influence of the time-varying orbital environment on the detectors.

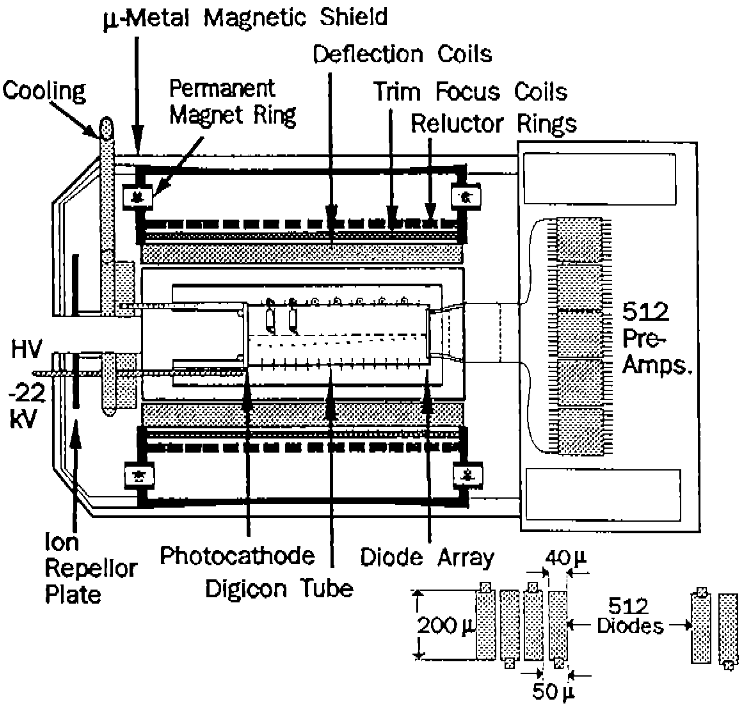

Figure 2. FOS detector layout with diode array

Each detector assembly is comprised of an FOS Digicon tube[9] (15cm in length), a reluctor ring type permanent magnet focus assembly (PMFA)[10] to provide a 105 gauss focusing field and external magnetic field shielding, magnetic deflection coils to scan the photocathode electron image across the target silicon diodes, and a set of 512 charge-sensitive preamplifiers to detect the pulses produced when the 22 keV photoelectrons strike the diodes. The target is a linear array of 512 silicon diodes on a 50 micron pitch with each diode 40 by 200 microns in area. Digicon target readout into digital buffer memory occurs as the photon events arrive, to within several microseconds, with readout virtually noiseless at ~10^{-5} false counts per diode per second. To develop a spectrum, a repetitive pattern of deflection steps is performed where the photon events from the array are accumulated in the buffer memory for a frame time (user-set from 20 to 500 milliseconds) at a particular deflection step and then shifted and co-added into the appropriate elements of the image array in microprocessor memory. For example, for the UM675 spectral observation mentioned in section 1, the primary deflection pattern is a series of 20 consecutive deflection steps of 1/4 pitch (12.5 microns) each in the diode array axis (spectral dispersion direction). Each 1/4 step deflection is 250 milliseconds in duration. This pattern is then repeated until completion of the 2000 second exposure segment. In addition every 250 seconds during the exposure segment the accumulated spectral image is read out of the FOS microprocessor memory for any *post facto* ground corrections. The 1/4 stepping format is performed to fully sample the Digicon point spread function and to avoid data aliasing problems. Additionally the 1/4 stepping pattern is carried on over 5 diodes (20 deflection steps) in order to fill in gaps in the spectrum that would normally be lost by non-functional diodes, preamplifiers or amplifiers, and also to average out any variation in sensitivity between target diodes.

In the FOS Digicon tubes, photoelectrons are accelerated from the semi-transparent photocathode toward a silicon diode array. The accelerating potential is around -22 KV. To focus the photoelectrons, there is a magnetic field of 105 gauss parallel to the electric field. The field parameters are chosen so that the photoelectrons execute exactly one full gyro-loop in the time it takes to travel from the photocathode to the diode array. The electron motion is basically along the magnetic field lines. If an external field is added to the focus field, then the image shifts by the amount that the magnetic field shifts. There is an additional small motion perpendicular to the total magnetic field that results from the non-parallel component of the electric field. Because each photoelectron completes one gyro-loop, in plasma physics terms, it is only necessary to consider the guiding center motion. For the FOS parameters this E x B drift produces a 17.8° rotation of the deflection axis.

A magnetic shield is attached to the exterior of the detector assembly to attenuate the Earth's dipole field variation during the orbit. As diagramed in Figure 2, the FOS magnetic shield is a standard 2-layer design with an outer layer of 0.32 inch thick Co-netic high permeability ($\mu \sim 10^5$) material and an inner layer of soft iron material of lower permeability ($\mu \sim 5 \times 10^3$), both separated by a gap of nonferromagnetic material. The FOS detector shield attenuation specification is 140, the value measured in test labs for the FOS prototype detector. At this specification a 0.5 gauss orbital change in the Earth's magnetic field would be attenuated to 0.0035 gauss and move the FOS image by 5 microns.

Since the exterior surface of the detector faceplate floats at the -22 KV Digicon operating voltage, an ion-repelling plate is attached to the front of the detector assembly. An ion plasma density of about 10^5 cm^{-3} of mainly O^+ ions with 0.2eV average thermal energy is expected at the HST altitude[11]. The ion plate shown in Figure 2 is set at a plus 14 volt potential and is designed to repulse any positive ions that manage to work their way into the deeply buried FOS Digicons; otherwise detector background would be considerably increased. Fortunately no problems have been seen associated with the FOS detector high voltage system in the orbital environment and this topic will not be discussed further.

Modeling during the FOS design phase indicated that most of the detector noise on orbit would be caused by cosmic ray particles depositing energy in the Digicon faceplate. The character of this noise was believed to be the essentially instantaneous formation of counts on many diodes. To suppress this burst noise, each 512 diode readout buffer frame is summed and accepted into the accumulated microprocessor array image or rejected based on whether the sum is smaller than a preset limit count. The FOS frame buffer time can be set short enough that for faint objects no more than 1 count per frame per array occurs with most frames having no counts. Then the relatively infrequent Cerenkov bursts that cause multiple counts in a frame can be effectively rejected with minimal signal loss. The FOS detector background specification is 0.002 counts per second per diode.

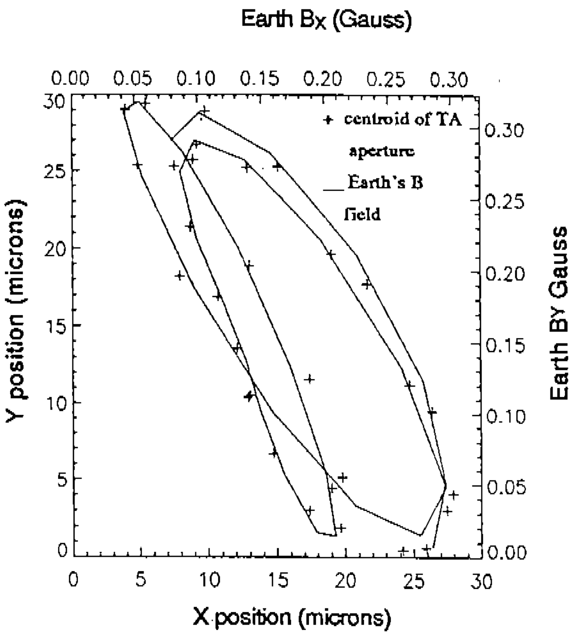

Figure 3. TA aperture movement over an orbit for Red Digicon

3. FOS DETECTOR IMAGE STABILITY

For short exposures the FOS detector resolution in the direction parallel to spectral dispersion is about 50 microns, which is unchanged from ground test values; however a careful study of the 0.3" FOS entrance aperture and spectral line positions with time indicates a larger than expected geomagnetically induced motion in the FOS detector images. Evidently the FOS detector mu-metal shields do not adequately attenuate external magnetic fields. Figure 3 (pluses) displays the physical movement of the centroid of the 0.3 arcsec diameter circular FOS entrance aperture as measured by the Red detector during several orbits. Fortunately the amplitude of geomagnetically induced motion problem (GIMP) in the Blue detector is about 4 times less than that shown for the Red detector and FOS Blue side performance is not significantly affected by GIMP.

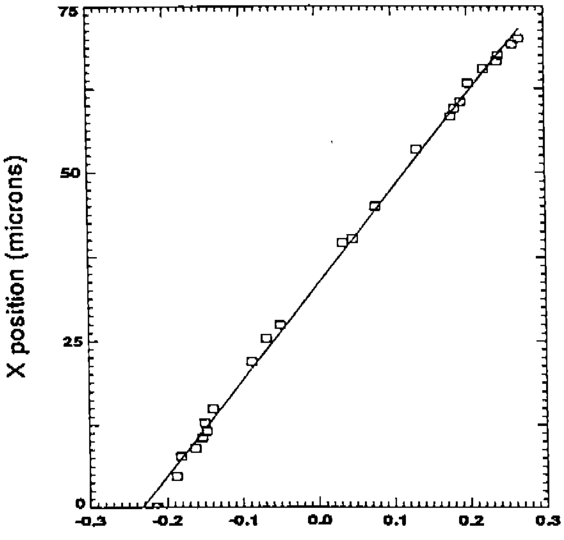

Figure 4.UM675 grating zero order centroids

Left uncorrected, the Red detector geomagnetically induced drift could cause significant spectral resolution degradation for the typically long, multiorbit, FOS science exposures. This effect has been studied in detail and a technique has been developed for removing geomagnetically induced image motion from FOS science data[12]. Since FOS science data are read out every few minutes during a science observation, each differential readout can be recentered during data-reduction processing according to the computed shift determined by the geomagnetic image motion model. The deflection in the FOS Digicons is expected to be primarily correlated with B_X, the component of the B-field parallel to the direction of interest. This assumes that the ferromagnetic materials in the FOS instrument and HST, the FOS detector magnetic shield and the permanent magnets, do not distort the contribution from an external B-field, but merely attenuate it. We will show that there is little or no distortion. As mentioned in section 2, there is also an E x B drift which introduces a $0 = 17.8^\circ$ rotation so that in the x direction:

$$\Delta x = G\,(B_X \cos\theta - B_Y \sin\theta), \qquad (1)$$

where Δx is the x deflection and G is a constant which depends on the amount of attenuation provided by the magnetic shield. We used the International Geomagnetic Reference Field (IGRF) model[13] for calculation for the Earth's B-field for each readout orbital position. A computer program does the transformations to find the magnetic field components in the coordinate system attached to the Digicon. The solid line in Figure 3 is the Earth's magnetic field for the orbit from the IGRF model transformed to the Digicon image plane and overlaid onto the FOS entrance aperture position data. The near-exact correlation between the aperture position and Earth's B-field is evident.

Some of the data taken with the FOS can be self-aligned by using intrinsic spectral features such as the grating zero order. This technique was used to effectively remove the GIMP smear from the HST early science observation of the faint QSO UM675. In Figure 4 the centroid of the zero order feature for every 250 second subexposure readout for the UM675 spectral observation is plotted as a function of transformed Earth's B-field. Again a linear function fits the centroid positions with an RMS deviation of 1.2 microns for this multi-orbit (see Figure 1) observation. The sensitivity coefficient fit derived from the UM675 zero order data is 143 microns per gauss.

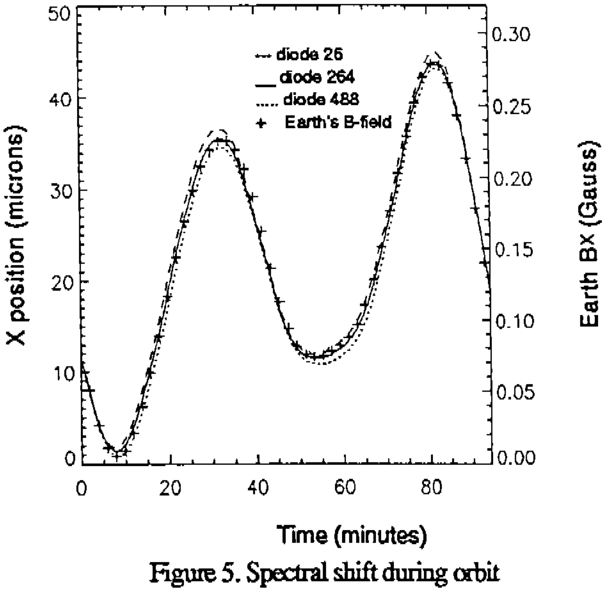

Figure 5. Spectral shift during orbit for Red Digicon

Recently a special series of FOS internal tests were run to determine the limiting accuracy associated with this GIMP model correction technique. HST GIMP Proposal ENG3138 is comprised of two FOS setup modes: first a sequential

TABLE 1. GIMP factors for different pointings

Pointing (RA, DEC)	Mode	GIMP (micron/gauss)	RMS deviation (microns)
0,-90	spectral	150.5	1.40
0,-90	aperture	88.5	1.60
0, 90	spectral	144.5	.55
0, 90	aperture	86.5	1.55
180, 0	spectral	156.5	.65
180, 0	aperture	93.0	.86
90, 0	spectral	148.5	.75
90, 0	aperture	93.5	1.20
average	spectral	150	----
average	aperture	90	----

repetition of standard spectral scans as would occur during a science observation, although in this case using the internal FOS spectral calibration lamps; and then a repetition of Target Acquisition maps of the internally illuminated 0.3 arcsec entrance aperture. Each of these two setups was run at four orthogonal pointing directions in order to look for any dependence of the GIMP factor "G" on HST orientation. The results from this series of tests, shown in Table 1 , give the average spectral GIMP factor of 150 microns/gauss ±6 microns/gauss. This uncertainty in the spectral GIMP factor introduces a worst case ±3 micron uncertainty in spectral line position for a 0.5 gauss orbital change in the Earth's magnetic field.

Figure 5 shows the (180, 0) spectral centroid data from Table 1 for the two edges and middle of the array as a function of time. Overplotted (as pluses) is the GIMP model fit at the 156.5 microns per gauss sensitivity factor with the Earth's magnetic field scale on the right side of the plot. The maximum deviation of only several microns across the array is typical of the other 3 pointings and indicative of a very uniform deflection field characteristic, evidently free of serious field distortions associated with nonuniform permeable material. This shows that our previous assumption was correct.

There are several good reasons why this GIMP correction technique works better than one might expect. The Earth's magnetic field is used in spacecraft stabilization and is extremely well modeled and stable for the HST near-Earth orbital region. Secular variation of the Earth's dipole moment is only 0.4%/year and programmed into the computer field models; solar flare induced magnetic storms produce only on average a hundred gamma (0.01 gauss) variation in the Earth's quiescent field[13]. Also, very little of the HST spacecraft is composed of heavy, field-distorting, ferromagnetic material.

GIMP introduces a photometric problem not corrected by shifting the data in the spectral "x" direction. Although the FOS Digicon diodes are 200 μm high, the drift perpendicular to dispersion can cause a small part of the HST aberrated image in the large aperture to miss the diode array. Since this effect is difficult to remove by calibration, these losses of several percent of the signal will affect high signal to noise photometry and spectral polarimetry. For this and other reasons a real-time GIMP correction has recently been implemented where the Earth's magnetic field is nulled by the FOS detector deflection coils. The details of this elegant procedure for GIMP removal are discussed in the paper by Fitch, *et al.* entitled, "Correcting the GIMP on the HST's FOS," in these proceedings.

Although the GIMP factors for each mode are remarkably stable, it is obvious from Table 1 that the aperture map and spectral scan GIMP factors significantly differ by some 40 percent. This difference is seen in all FOS observations. Clearly the GIMP model can be implemented without knowing the cause of this difference by using a mode dependent GIMP factor. However, to understand the reason for the mode-dependent GIMP factor difference, we set up a spare FOS Digicon in a UCSD laboratory and ran further tests to uncover the cause. The results of these measurements are discussed in the next section.

3.1 Laboratory measurements

During development of the HST detectors, it was discovered that after large currents to the Digicon x and y deflection coils, the image would return to a slightly offset position from the original starting location. The problem was

TABLE 2. Average Size of the Image Shift for Various Degauss Spacings for FOS Spare Blue Detector

Degauss Spacing (gauss)	Degauss Jump (microns)
0.031	3.22
0.062	4.14
0.186	11.96
0.310	18.75
0.620	38.10

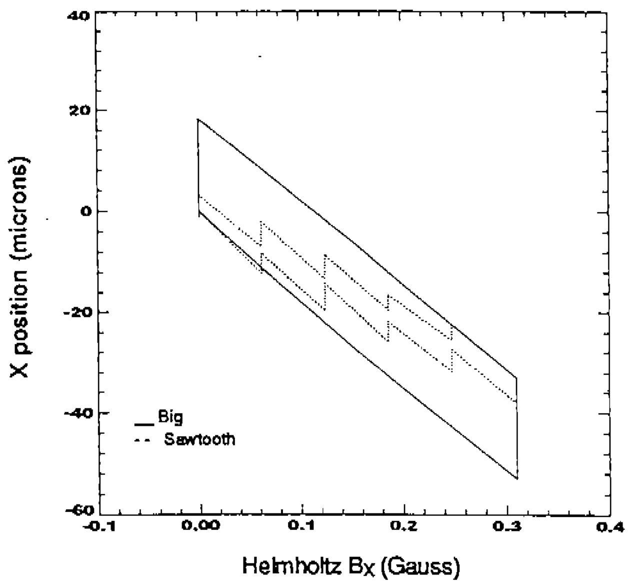

Figure 6. Degauss jump simulation

determined to be hysteresis in the reluctor rings of the PMFA structure. To overcome this unacceptable variation of the image origin, a degauss procedure is perfomed after large deflection. For the FOS instrument the degauss procedure consists of a spiral to zero deflection starting from 4096 deflection units. Each reduction at the end of an individual spiral is by 128 until 2176 is reached, then the deflection is reduced by a factor of 2 until 2048 is reached. The FOS degauss pattern performs in about 0.5 second. Note that 0.0 deflection current is a setting of 2048 into the deflection coil digital to analog converter and that 1 D to A deflection step of 0.0011 gauss moves the Digicon image 1.6 microns.

It happens to turn out that the major difference between the TA aperture scans and spectral scans is the frequency of performing this degauss pattern. The spectral scans as with the science observations have only a single degauss pattern performed just before the start of the 96 minutes of sequential spectral scans. However for the TA aperture scans a degauss pattern is performed before each sequential aperture scan at a rate of a degauss every 3 minutes.

In order to verify that the frequency of degauss patterns is the cause for the GIMP factor variability, we set up an external magnetic field laboratory test. The FOS spare Blue detector was situated in the middle of two 42 inch diameter coils that were 21 inches apart, producing a uniform parallel field. The Helmholtz coil field was oriented parallel to the diode array and the axis of the PMFA was oriented parallel to the Earth's magnetic field in order to minimize its effects on these measurements. An optical projector imaged a long slit onto the Digicon photocathode; the slit's long axis was oriented perpendicular to the diode array. This produced a 70 micron wide focused beam of light at the Digicon photocathode that covered the entire height of the diode array, so all Y locations yielded the same central X location.

The most illustrative of the tests taken with this FOS spare Blue detector setup are shown in Figure 6. The SAWTOOTH scan shown in Figure 6 is a degauss every 0.062 gauss up to 0.31 gauss with positional measurements every 0.031 gauss; this pattern is then reversed to 0.0 gauss. The BIG data set shown in Figure 6 is a single degauss at 0.31 gauss with positional measurements at 0.155 and 0.31 gauss; this pattern is also reversed down to 0.0 gauss. Note that after a degauss, the shift in image position always resumes the "no degauss" GIMP factor "G", which is the slope of the traces in Figure 6. The degauss simply changes the starting position. In addition, the multi-degauss SAWTOOTH pattern ends up at the same location as the single degauss in BIG. We have measured the average degauss "jump" for various degauss spacings. The results are listed in Table 2 and the data are fit nicely by a straight line with a slope 57 microns/gauss which we call the "Degauss Factor".

Thus a single constant still fits our data to the variation of the Earth's magnetic field. However this new factor is simply the "no degauss" GIMP Factor minus the Degauss Factor. In the TA section of the SV GIMP proposal, the degauss occurred every 3 minutes with a resulting anomalous GIMP coefficient of 90 microns/gauss. The 60 microns/gauss average difference between the aperture and spectral GIMP factors in Table 1 corresponds closely to the 57 microns/gauss value determined in these lab tests.

Note that both GIMP and degauss jumps are about what one would expect from the theory of ferromagnetic material[14] and came to our attention because the shield on the orbiting Red detector doesn't work very well. In fact one reference[15] recommends designing shielded magnetic field free regions with internal coils (such as the FOS deflection coils) so that a degauss pattern can be performed. This reference says that an internal degauss in effect improves the magnetic shield by removing the induced magnetization field originating from the surrounding shield structure. Evidently without continuous degaussing, the residual PMFA field caused by the aligning of the magnetic domains along the Earth's magnetic field lines is usually adding to the Earth's field component and enhancing the Earth's field deflection effect in the Digicon.

3.2 FOS magnetic shield details

The PMFA structure included the magnetic shield (see Figure 2) and was procured as a complete unit. The procurement specification for external field attenuation factor "A" is 140. Years of ground-based telescope science observations demonstrated the importance of a good magnetic shield around the Digicon detector. The ground-based Digicons were generally mounted at the Cassegrain focus of the telescope and, of course, would move relative to the Earth's field as the telescope tracked. The shields were manufactured from 3 stacked layers of progressively higher permeability mu-metal. The attenuation factor for these ground-based telescope Digicon shields was about 100.

A Figure of merit for the the detector external field sensitivity "G" to image motion caused by an external magnetic field is given in microns per gauss from the formula

$$G = L/(A \times F) \qquad (2)$$

where F is the Digicon focus field of 105 gauss and L is the tube's photocathode to diode target length of 15 centimeters. Substituting the FOS magnetic shield attenuation specification of A=140 into formula 2, gives an external field sensitivity G of 10 microns per one gauss of external magnetic field change.

Our orbital FOS data for the Red detector image motion from spectral science data (Figure 4) indicates that for the Red detector, G=150, so A=10. However the orbiting Blue detector is somewhat better with G=35 and A=41. The first set of magnetics developed for the FOS project was used in the Design Verification Unit (DVU). This unit was extensively tested by the FOS prime fabricator with the result of A=140 for the DVU.

The build history of the four PMFA flight units is as follows. The orbiting Blue detector PMFA in the HST was fabricated in the original 1980 flight build. However the orbiting Red detector PMFA in the HST was fabricated in the spares flight build in 1985; a photocathode problem with the Red Digicon tube then installed in the FOS required a detector replacement with its spare in 1987. The spare Blue detector PMFA in storage was fabricated in 1985. The spare Red detector PMFA in storage was fabricated in 1980. Both PMFAs built in 1980 were tested for external field attenuation and found to be within specification. Although the PMFAs built in 1985 were not measured for external field attenuation at the time of fabrication, all material and processes from the fully tested 1980 build were used for the 1985 fabrication.

Recent measurements at UCSD, using the laboratory Helmholtz coils setup on our stored FOS detectors, indicate the stored Blue detector (with 1985 magnetics) sensitivity to external fields is 167 microns per gauss with a calculated attenuation factor of 8.6. The stored Red detector sensitivity factor is closer to specification at 14 microns per gauss with a calculated attenuation factor of 102. Here, the attenuation calculated from equation 2 is derived from the image shift caused by a known field developed by the surrounding Helmholtz coil setup.

A possible cause for the loss of shield performance in the 1985 magnetics is that the shields were manufactured slightly undersized in diameter for that 1985 fabrication. In order to slip the shield (basically a mu-metal cylinder) onto the PMFA structure (another smaller diameter cylinder), the shield had to be hammered into place with a rubber mallet. This first came to our attention only recently. To be an effective magnetic shield, mu-metal must be annealed. This procedure is done on the shield before installation onto the PMFA, since annealing requires a temperature cycle up to ~1200°C in a hydrogen furnace. Unfortunately, any sharp impacts on annealed mu-metal can reverse the annealing process and degrade the performance of the shield to reject external magnetic fields. So it is likely that for the 1985 vintage the shields were seriously degraded during the hammering placement onto the PMFAs. The self-shielding from the PMFA ferromagnetic material without the mu-metal shield is measured in the lab to be A~7, compared to A=10 with the shield; it is evident that the 1985 magnetic shields are not very functional at about fifteen times below specification.

An additional factor accounting for some loss of shield performance in the orbiting Blue detector is a little-known temperature derating factor. In orbit the PMFA operates at -15° Centigrade, whereas the FOS ground shield attenuation measurements were performed at room temperature. However the mu-metal shield performance can be expected to be reduced by as much as 40% by this 40°C cooler operating point [16].

It should be mentioned that except for this shield problem, the overall performance of the PMFAs is excellent. The PMFAs deliver a stable 105 gauss field, uniform to better than 1%.

4. FOS ORBITAL DETECTOR BACKGROUND

During the extensive ground test activity, the FOS detectors registered about $4*10^{-4}$ cts s^{-1} d^{-1} noise levels when operated at high voltage. However in the near-Earth orbit of the HST, the radiation environment considerably elevates this level to around 0.01 cts s^{-1} d^{-1}. High energy particles generate light in the faceplate by the Cerenkov, fluorescence, and phosphorescence processes[17].

An additional source of detector noise could occur when a cosmic ray travels through the Digicon target array and preamplifier field effect transistors, creating a pulse of electron-hole pairs in the silicon substrates. FOS orbital background observations with the Digicon high voltage setting at zero volts yield a background of $\sim 3x10^{-4}$ cts s^{-1} d^{-1}, demonstrating that the Digicon target and readout electronics are insensitive to cosmic rays.

Although the FOS operates safely at high voltage during an SAA passage, generally no science observations are performed there because of the high background. The contour in Figure 1 centered around "SAA" is at about .02 cts s^{-1} d^{-1} background level and defines the region of non-science activity for observations of faint objects. Peak FOS detector background rates in the center of the SAA contour are around 1.0 cts s^{-1} d^{-1}.

Rosenblatt *et al.*[18] have modeled the background data for the FOS Blue detector in detail and found that the predominant source of orbital noise comes from Cerenkov light generated by cosmic rays transiting the faceplate. On average, a single cosmic ray proton passing through the Digicon's 3/8th inch thick by 2 inch diameter faceplate results in the essentially instantaneous burst of several thousand Cerenkov photons onto the Digicon photocathode. Fortunately, only about 14% of the cosmic rays that transit the faceplate cause diode events in the detector array, due to geometric dilution and other attenuation factors.

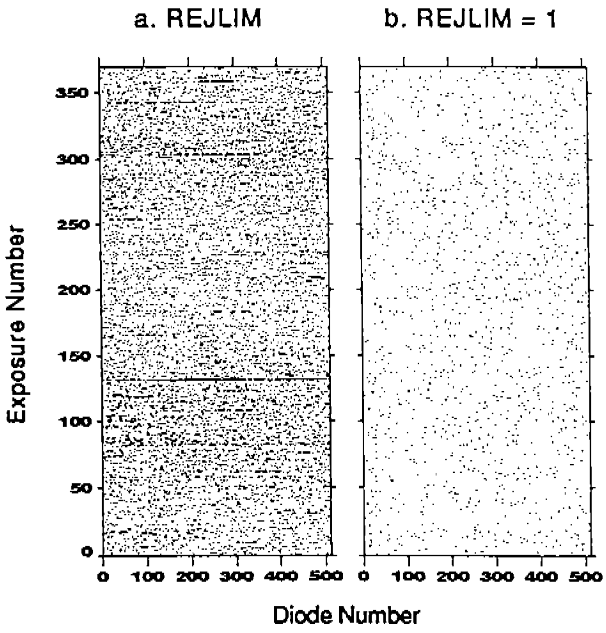

Figure 7. Image plot of Red side noise

Figure 7a shows a Red detector image for a 1840 second observation spread out over 63 minutes of orbit. The diode number is plotted along the x-axis and exposure number along the y-axis (proportional to time) with a count represented as a spot in the Figure. Each exposure line is 5 seconds in duration. Long streaks of diode hits (most likely due to faceplate Cerenkov radiation from cosmic rays) are clearly apparent. Note also the modulation of the average background level with time due to the cosmic ray geomagnetic latitude effect mentioned in section 1 seen in broad increases centered at exposure 80 and 320.

The count rate for the FOS observation of the faint QSO UM675 is about 0.01 cts s^{-1} d^{-1} near 1850Å, roughly equal to the detector background rate. The detector subtraction background function is determined by summing many previously acquired dark exposures. For a typical long FOS accumulation, the unusual event statistics shown in Figure 7a average out to a fairly unifom response across the array, with diode-to-diode fluctuations determined by counting statistics. This background function is then scaled to match the signal found between the first and zero order, a region devoid of UM675 signal, and subtracted from the UM675 spectrum.

The FOS orbital background noise can be reduced by setting the burst rejection limit (REJLIM) algorithm mentioned in section 2 in order to edit out a percentage of the Cerenkov flashes. Figure 7b shows FOS background data for the same setup conditions as shown in Figure 7a except that REJLIM is set to 1. At the lowest meaningful setting of REJLIM=1 (rejection of FOS 250 ms image frames with 2 or more counts), the dark count is reduced to 20% of the normal background and meets the FOS background specification of 0.002 cts s^{-1} d^{-1}, improving the FOS limiting magnitude performance.

5. FOS PHOTOMETRIC STABILITY

Absolute photometric SV calibrations were perfomed by observing standard stars with the results for the FOS high resolution (R=1200) gratings shown in Figure 8. Overlaid on Figure 8 are the GHRS low resolution (R=2000) and medium resolution (R=20,000) calibration to show the degree of safety overlap between the FOS and GHRS instruments after launch. The sensitivity of the FOS instrument was essentially unchanged from prelaunch expectations, except in the region shortward of 1500Å where the sensitivity factor gradually drops below prelaunch estimates until it reaches a factor of 2.5 lower than expectation at 1200Å. Initially this was thought to be associated with a thin film contaminating the exterior of the Blue Digicon MgF faceplate. However a comparison of the wavelength dependence of this short wavelength decay indicates that it is due to a growth of an aluminum oxide layer on the grazing incidence mirror. In order to minimize interference effects that would be caused by a 78° reflection off a coated mirror, this mirror was not coated with the typical MgF protective layer. Evidently the extended HST launch delay from 1983 to 1990 lead to enhanced atmospheric oxidation of this unprotected aluminized reflector. Hopefully the HST refurbishing mission in late 1993 will restore Side 1 GHRS operation so that the GHRS low resolution mode can be used to more effectively cover this short wavelength region.

The FOS Blue side shows little structure or "granularity", with standard deviation typically about 1-2% of the mean for each grating, and has a few strong blemishes with σ >5%. Continuing Blue side measurements show an overall loss of sensitivity of up to 10% in 1991, with a smaller degradation rate in 1992. This Blue side sensitivity loss is relatively wavelength independent. However, the only Digicon degradation effect seen in extensive laboratory lifetime tests was a characteristic long wavelength decay in quantum efficiency presumably associated with an

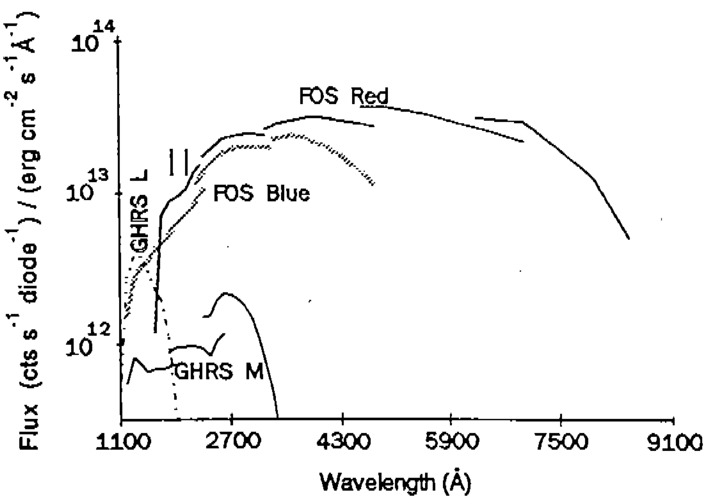

Figure 8. Flux calibration of FOS and GHRS instruments

increase in the photocathode work function [19]. At this time it remains under investigation whether the Blue side loss in efficiency is associated with the detector or the FOS feed optics.

The Red side measurements indicate that the sensitivity is stable to within 5% overall, with an exception in the 1850Å to 2050Å region, where an absorption dip of ~15% centered at 1950Å developed in 1991; the rate of sensitivity loss slowed in 1992. The spectral character and amount of these sensitivity losses are indicated in Figure 9 and the bracketed region in Figure 8 puts this absorption feature in perspective. The lower unprocessed spectrum in relative cts s^{-1} d^{-1} of Figure 9 is a December 1990 observation of the IUE photometric calibration star BD28°4211. Note that the abrupt drop off shortward of 1700Å is due to the Suprasil faceplate cutoff. The upper plot in Figure 9 is a division of a September 1991 observation of BD28°4211 by the December 1990 observation. The region shows strong (5-15%) granularity increasing with time, and marked temporal variations. This apparent absorption feature is likely detector related and was thought to be due to the formation of color centers in the Digicon Suprasil faceplate[20] caused by SAA radiation damage; but a test of a spare faceplate at a particle accelerator has not confirmed such an effect [21]. Two other possible explanations under investigation for the 1950Å absorption feature are (1) a thin film contamination on the external surface of the Digicon faceplate and (2) a photocathode aging process.

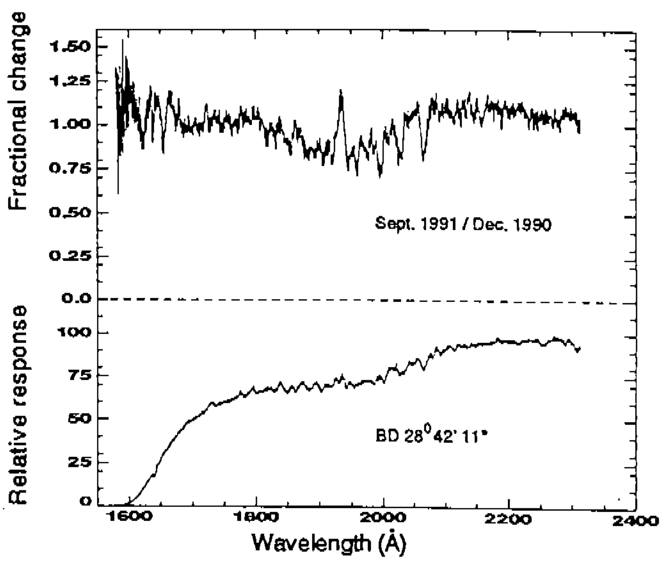

Figure 9. Flat field calibration with later 1950Å dip development

This 1950Å feature is effectively removed from FOS Red side data by updating the FOS calibration data base with monthly observations of spectrophotometric standard stars. The standard stars such as BD28°4211 possess known, fairly uniform flux distributions, making them ideal for removing instrumental features. At the time of the early UM675 observation, the presence of the 1950Å feature was unknown; fortunately the UM675 observation was flux calibrated and flat-fielded using an observation of a standard star made the previous day.

During the 10 year development of the FOS instrument, a serious recurring problem with the Red Digicon was the slow long wavelength quantum efficiency decay caused by cesium migration off the S20 photocathode. Evidently the photocathode processing technique developed to solve this problem[19] was successful since the long-wavelength response of the Red detector remains unchanged from 1987 fabrication values.

6. FOS OBSERVATIONS

The HST was designed to make high spatial resolution observations which would be impossible from the ground, for example achieving detection of faint objects such as variable stars in external galaxies by excluding the contaminating background light. It serves another purpose as well, performing UV observations, which can only be made above the atmosphere.

Unfortunately, the well-known spherical aberration of the HST primary mirror has seriously affected the ability of the HST to perform its mission, particularly where high spatial resolution is required. For UV spectroscopy and spectropolarimetry, however, the HST can reach most of its intended scientific objectives, albeit with considerably longer integration times. The longer integration times are required because a substantial fraction of the light is lost through the small apertures; these apertures were designed with the high spatial resolution capabilities of the HST in mind. The spectroscopic capability of the HST will be almost completely restored after the installation of the corrective optics contained in the COSTAR in late 1993.

Despite the spherical aberration, the launch of the HST on April 24, 1990 ushered in a new era for ultraviolet spectroscopy, as the light gathering power of the HST far exceeded that of any previously launched UV sensitive instrument. The previous UV workhorse has been the International Ultraviolet Explorer (IUE), but the spectrographs on board the HST are capable of observing much fainter objects than the IUE, and at higher resolution. As the name implies, the FOS is designed for low and moderate resolution spectroscopy of faint objects with resolution of R=200 and R=1200 respectively. The FOS low resolution mode is similar in resolution to the IUE low resolution mode, but can be used to observe objects more than three magnitudes fainter than the IUE limit. Although the IUE has a high resolution mode, this has been used to observe only one QSO! The IUE has no observation mode similar to the FOS high resolution mode.

Some of the greatest advances are coming in the study of quasi-stellar objects (quasars or QSOs); the FOS opens up new areas in spectral resolution and signal-to-noise. The QSOs are probably super-massive black holes at the cores of galaxies; they show both emission and absorption features (see Figures 10 and 11). Gas in rapidly moving clouds near the central black hole gives rise to the emission lines; gas along the line of sight to the QSO gives rise to the absorption lines.

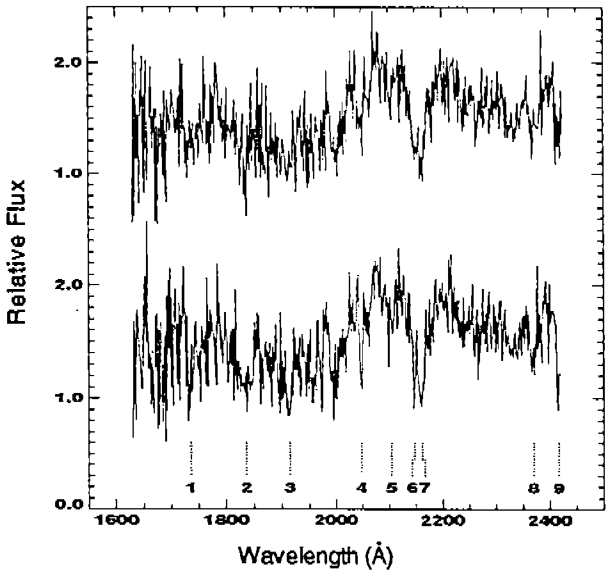

Figure 10. Before (top) and after GIMP correction on UM675 Spectrum

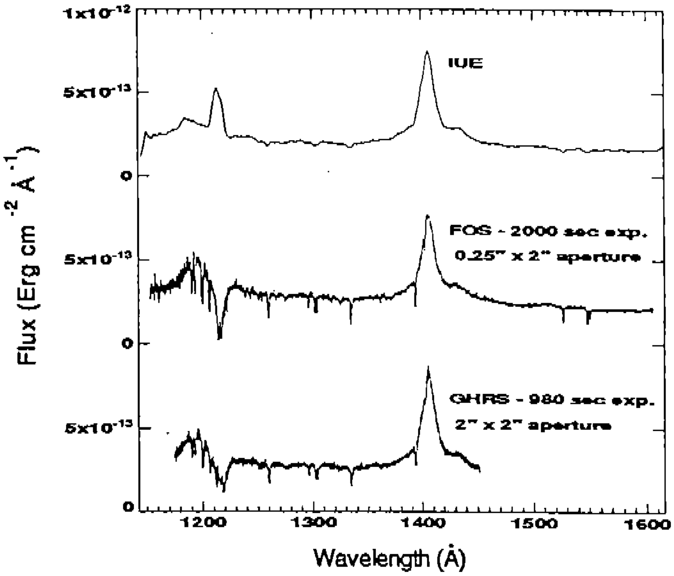

Figure 11. 3C 273 - Comparison of IUE, FOS and GHRS

Considerable optical telescope time has gone into the characterization of the absorption line spectra of QSOs. These absorption lines are primarily assigned to "metal-line" systems or the Lyman α forest. The former are probably related to galaxies along the line of sight, while the latter may be caused by absorption in primordial intergalactic hydrogen clouds. Most of the observational work prior to the launch of the HST had been done at high-redshift only, because the lines at low redshift (the last 7 billion years or so) are in the UV, and not accessible from the ground.

UM675 (Figure 10) is an example of low resolution spectroscopy with the FOS[22]. This object is undetectable with IUE. This observation was a total of 100 minutes divided among three successive orbits. Long observations must be broken into sections because of interruptions due to Earth occultation and passage through the SAA. Each section is read out every few minutes as well. This allowed us to make a *post facto* correction for the shift of each read out.

The effect of GIMP on spectra is primarily one of decreasing the spectral resolution. In Figure 10 we have marked the absorption lines we detect in this spectrum. The upper spectrum is the uncorrected spectrum. In the lower spectrum, each of the 24 individual 250 second spectra has been shifted to align the zero order spectrum present in the low resolution observations. This method was used prior to the development of the GIMP model and yielded 143 μ/gauss, similar to the result derived from the model. It is apparent that all absorption lines are much clearer in the corrected spectrum than in the original.

Line 7 is probably Lyman α at $z=0.78$; metal lines in this system are previously known from optical observations. Line 9 is a line of Ne VIII in a cloud which may be associated with the QSO itself; absorption lines with an ionization this high had not previously been detected in a QSO spectrum. Lines 3, 4, and 5 are probably Lyman α forest absorption lines. If so, they are unexpectedly strong; extrapolation from the optical observations would predict fewer than one line of this strength in this redshift range. This was the first suggestion of a rich Lyman α forest at low redshift.

The high density of lines at low redshift is shown more clearly in the spectrum of 3C 273. 3C 273 is the optically brightest QSO. The IUE low resolution spectrum[23] is shown in Figure 11 along with the FOS high resolution spectrum[24] and GHRS low resolution spectrum[25]. Although the multi-hour IUE spectrum appears to be quite high signal-to-noise, the FOS high resolution spectrum shows many absorption lines. Most of the lines in this spectrum are resonance lines of metals in our Galaxy. The rest are probably Lyman α forest lines[24,25]. At high redshift, there are many more lines but the number density falls off rapidly at lower redshifts. If the lines in 3C 273 are Lyman α lines, then there are a factor of 5 to 10 more than would be expected by extrapolating the number density from high redshift. A possible explanation is that the density of ionizing photons in the universe drops steeply below a redshift of two[26]; this is consistent with the fall in the number density of the QSOs themselves.

7. ACKNOWLEDGMENTS

It is a pleasure to acknowledge the years of work from the talented individuals of the FOS fabricator, The Martin Marrieta Corporation. Additionally the Digicon tube manufacturer, Science Applications International Corporation, and Hank Wenzel deserve praise for fabricating Digicon electron tubes that continue to survive the rigors of space and orbital science operations. Dr. Norm Dionne of the Raytheon Corporation graciously attempted to educate us on the subtleties of magnetic structures. Thanks to Paul Foster for GIMP laboratory testing and Mark Loveland for dragging us into the world of desktop publishing. This work has been supported by NASA Contract NAS5-24463 and Grant NAG 5-1630.

8. REFERENCES

1. R. J. Harms, R. Angel, F. Bartko, E. Beaver, W. Bloomquist, R. Bohlin, E. M. Burbidge, A. F. Davidsen, J. C. Flemming, H. Ford, B. Margon, "Faint Object Spectrograph for Space Telescope", *Proceedings of SPIE*, 183, p. 74-87, May, 1979.

2. U.S. Patent 3,798,453 by C. E. McIlwain and E. A. Beaver, 1974.

3. E. A. Beaver and C. E. McIlwain, "A Digital Multichannel Photometer," *Review of Scientific Instruments*, 42, p. 1321-1324, 1971.

4. E. A. Beaver, R. J. Harms, G.W. Schmidt, "Digicon Applications in Astronomy," in *Advances in Electronics and Electron Physics*, 40B, p. 745-763, 1976.

5. R. J. Harms, J. R. P. Angel, F. Bartko, E. A. Beaver, R. Bohlin, E. M. Burbidge, A. Davidsen, H. Ford, B. Margon, J. McCoy, and L. Ripp, "Faint Object Spectrograph Calibration," *Proceedings of Society of Photo Optical Instrumentation Engineers*, 331, p. 268-278, 1982.

6. R. Harms, E. Beaver, E. Burbidge, R. Hier, R. Allen, R. Angel, F. Bartko, R. Bohlin, H. Ford, A. Davidsen and B. Margon, "Calibration and Operation of the Faint Object Spectrograph," *Proceedings of Society of Photo Optical Instrumentation Engineers*, 445, p. 410-426, 1983.

7. R. O. Ginaven, L. L. Acton, D. M. Dieball, R. B. Johnson, H. R. Alting-Mees, R.D. Smith, E. A. Beaver, R. J. Harms, F. Bartko, J. C. Flemming, J. G. McCoy, "Faint Object Spectrograph (FOS) 512-channel Digicon detector performance data," *Proceedings of SPIE*, 290, p. 81-89, June, 1981.

8. J. W. Haffner, *Radiation & Shielding in Space*, Academic Press, p. 289, 1967.

9. H. R. Alting-Mees, H. A. Wenzel, E. A. Beaver and J. L. Shannon, "Space Telescope Digicon," *Recent Advances in TV Sensors and Systems*, 203, p. 12-20, 1979.

10. C. I. Coleman, W. A. Delamere, N. J. Dionne, W. Kamminga, D. Long, J. L. Lowrance, and P. Van Zuylen, "Recent Developments in Permanent Magnet Focusing Assemblies for Image Intensifiers and Camera Tubes," *Advances in Electronics and Electron Physics*, 52, p. 89-99, 1979.

11. P. M. Banks and G. Kockarts, *Aeronomy* Part B, 204 , 1973.

12. V. T. Junkkarinen, E. A. Beaver, R. D. Cohen, R. Hier, R. Lyons and E. Rosenblatt,"Geomagnetic Image Deflection Problem in the Faint Object Spectrograph," *B.A.A.S.*, 22, p. 1282, 1990.

13. *Spacecraft Attitude Determination and Control*, edited by J. R. Wertz, 73., Reidel Pub. Co., Holland, 1978.

14. T. S. Scott, *The Physics of Electricity and Magnetism*, John Wiley, p. 352, 1959.

15. S. M. Freake, S. M. and T. L. Thorp, "Shielding of Low Magnetic Fields with Multiple Cylindrical Shells," *The Review of Scientific Instruments*, 42, p. 1411, 1971.

16. "Materials and Fabrication Guide," *Magnetic Shielding Corporation, Perfection Mica Company Catalog*, Bensenville, ILL, 1991.

17. W. Viehmann and A. G. Eubanks, *Noise Limitations of Multiplier Phototubes in the Radiation Environment of Space*, NASA Technical Note D-8147, 1976.

18. E. I. Rosenblatt, E. A. Beaver, R. D. Cohen, J. B. Linsky and R. W. Lyons, "Cerenkov Background Radiation in Imaging Detectors," *Proceedings on Electron Image Tubes and Image Intensifiers II*, ed. I. P. Csorba, SPIE, 1449, p. 72, 1991.

19. E. A. Beaver, L. Acton, E. Dozier, D.Doliber, and H. Wenzel, "S-20 Photocathode Stability Considerations," *Advances in Electronics and Electron Physics*, 74, p. 347-358, 1988.

20. B. D. Savage, "Ultraviolet Photometry from the Orbiting Astronomical Observatory XX. The Ultraviolet Extinction Bump," *Ap. J.*, 199, p. 92-109, 1975.

21. W. Fowler (retired), Goddard Space Flight Center, private communication, 1992.

22. E. A. Beaver, E. M. Burbidge, R. D. Cohen, V. T. Junkkarinen, R. W. Lyons, E. I. Rosenblatt, G. F. Hartig, B. Margon, and A. F. Davidsen, "Far-Ultraviolet Spectroscopy of the Quasar UM675 with the Faint Object Spectrograph on the Hubble Space Telescope," *Ap. J Letters*, 377, L1-4, 1991.

23. A. L. Kinney, R. C. Bohlin, J. C. Blades and D. G. York, "An Ultraviolet Atlas of Quasars and Blazar Spectra," *Ap. J. Supp.*, 75, p. 645, 1991.

24. J. N. Bahcall, B. T. Jannuzi, D. P. Schneider, G. F. Hartig, R. Bohlin and V. Junkkarinen, "The Ultraviolet Absorption Spectrum of 3C 273," *Ap. J. Letters*, 377, L5-8, 1991.

25. S. L. Morris, R. J. Weymann, B. D. Savage, R. L. Gilliland, "First Results from the Goddard High-Resolution Spectrograph: The Galactic Halo and the Ly Forest at Low Redshift in 3C 273", *Ap. J. (Letters)*, 377, L21-24, 1991.

26. S. Ikeuchi and E. L. Turner, "The Evolution of the Diffuse Cosmic Ultraviolet Background Constrained by Hubble Space Telescope Observations of 3C273," *Ap. J. (Letters)*, 381, L1-4, 1991.